Journal of Solid State Chemistry **161,** 1–8 (2001)
doi:10.1006/jssc.2001.9209, available online at http://www.idealibrary.com on IDEAL®

Thermal Behavior and Crystal Structure at 435 K of the Mixed Rubidium Ammonium Sulfate Tellurate $Rb_{1.12}(NH_4)_{0.88}SO_4 \cdot Te(OH)_6$

Lilia Ktari,* Mohamed Dammak,* Tahar Mhiri,* and Jean-Michel Savariault†

*Laboratoire de l'Etat Solide (L.E.S), Faculté des Sciences de Sfax, Universite de Sfax, Route de soukra, 3018 Sfax, Tunisia; and †Centre d'Elaboration de Matériaux et d'Etudes Structurales (CEMES), CNRS, Toulouse, France

Received December 16, 2000; in revised form April 4, 2001; accepted April 12, 2001; published online July 26, 2001

Crystals of $Rb_{1.12}(NH_4)_{0.88}SO_4 \cdot Te(OH)_6$ (RNST) have been prepared in an aqueous solution of H_6TeO_6 and the corresponding sulfates. The old parameters and space group found at room temperature are rectified. Indeed, at high temperature, the structure crystallizes in the monoclinic system, space group $P2$. The lattice constants are determined as follows: $a = 7.541(4)$ Å, $b = 6.772(4)$ Å, $c = 10.142(6)$ Å, $\beta = 98.03(2)^\circ$, $V = 512.8(5)$ Å^3, $Z = 2$, $D_x = 2.91$ g cm^{-3}, and $F(000) = 412$. The residuals are $R_1 = 0.037$ and w$R_2 = 0.082$, for 663 observed reflections refined with 82 parameters. The refined structure, at 435 K, shows that it is different from that obtained at room temperature, and the bond lengths differ from those obtained at room temperature. The structure is characterized by planes of mixed octahedra and tetrahedra, parallel to *bc* plane, and the cations Rb^+/NH_4^+ are intercalated between them. The structure is stabilized by two types of hydrogen bonds (O–H···O and N–H···O). The phase transitions of the mixed solution RNST are studied by differential scanning calorimetry and dielectric measurements. It is found that the transition occurs at 458 K to be ferro-paraelectric, whereas the peak at 483 K is attributed to the superprotonic conduction. This transition is confirmed by the conductivity measurements. © 2001 Academic Press

Key Words: **RNST material; rubidium compound; structure; DSC.**

I. INTRODUCTION

The compounds of general formula $M_nAO_4 \cdot Te(OH)_6$, where (M = Na, K, NH_4, Rb, Cs, A = S, Se, P and $n = 2, 3$) exhibit many interesting physical properties and phase transitions (1–4). Based compounds of the new mixed solution, which are $Rb_2SO_4 \cdot Te(OH)_6$ and $(NH_4)_2SO_4 \cdot Te(OH)_6$, are paraelectric at room temperature. Their symmetry can be described respectively by the monoclinic space groups $P2_1/a$ and Cc (5, 6). In previous papers, we have shown that controlled cationic substitution has a large effect on the structure of the host frameworks and induces important changes in the properties of the mother compounds.

The solid solution $Rb_{1.12}(NH_4)_{0.88}SO_4 \cdot Te(OH)_6$ structure, at room temperature, is being built of planes of pure tetrahedra SO_4 and planes of pure octahedra TeO_6. These planes are parallel to the *bc* one. The cations in this structure are intercalated in a bidimensional arrangement between these planes. The structure is stable thanks to network hydrogen bonds linking the anionic–anionic and cationic–anionic entities (O···O and N···O) (7). At 435 K, this compound shows a structural arrangement that is different from that obtained at room temperature and from those in $Rb_2SO_4 \cdot Te(OH)_6$ and $(NH_4)_2SO_4 \cdot Te(OH)_6$.

Dielectric studies performed on the RNST solid solution show that it presents a ferroelectric–paraelectric phase transition accompanied by a superprotonic conduction at high temperature (8).

In this paper, we report and discuss the results of investigations concerning the mixed compound $Rb_{1.12}(NH_4)_{0.88}SO_4 \cdot Te(OH)_6$ obtained by differential scanning calorimetry, dielectric measurements, and X-ray study at 435 K.

II. EXPERIMENTAL DETAILS

Colorless and transparent crystals of rubidium ammonium sulfate tellurate $Rb_{1.12}(NH_4)_{0.88}SO_4 \cdot Te(OH)_6$ were grown by slow evaporation at room temperature of an aqueous solution:

$$H_6TeO_6 + x(NH_4)_2SO_4 + (1-x)Rb_2SO_4 \rightarrow Rb_{2-2x}(NH_4)_{2x}SO_4 \cdot Te(OH)_6.$$

Rubidium, nitrogen, and sulfate contents were determined by chemical analysis; the quantitative result was subsequently confirmed by the single-crystal experiment.

0022-4596/01 $35.00

TABLE 1
Main Crystallographic Data for $Rb_{1.12}(NH_4)_{0.88}SO_4 \cdot Te(OH)_6$

Formula	$Rb_{1.12}(NH_4)_{0.88}SO_4 \cdot Te(OH)_6$
Formula weight	532.73
Crystal system	Monoclinic
a (Å)	7.541 (4)
b (Å)	6.772 (4)
c (Å)	10.142 (6)
β (°)	98.03 (2)
V (Å^3)	512.8 (5)
Z	2
Space group	$P2$
T (K)	435 (2)
Diffractometer	Enraf–Nonius Kappa CCD
θ_{max} (°)	29.88
λ (Mo$K\alpha$) (Å)	0.71069
ρ_{cal} (g cm^{-3})	2.91
μ (cm^{-1})	78.5
Total reflections	663
Reflection with $I > 2\sigma(I)$	542
Parameters	82
min., max., $\Delta\rho$ (e/Å^3)	-0.479, $+0.401$
R (F)[a]	3.7
Rw (F)[a]	8.2

[a] R values are defined as $wR_2 = (\sum[w(F_o^2 - F_c^2)^2]/[w(F_o^2)^2])^{1/2}$ and $R_1 = \sum||F_o| - |F_c||/\sum|F_o|$.

TABLE 2
Fractional Atomic Coordinates and Temperature Factors for $Rb_{1.12}(NH_4)_{0.88}SO_4 \cdot Te(OH)_6$

Atoms	x	y	z	U_{eq} (Å^3)	Occup.
Te(1)	0.0000	0.003(3)	0.0000	0.055(4)	0.5
Te(2)	0.5000	0.541(3)	0.5000	0.0229(8)	0.5
S(1)	0.0000	0.0440	0.5000	0.037(7)	0.5
S(2)	0.5000	0.497(5)	0.0000	0.031(4)	0.5
Rb(1)	0.964(2)	0.525(5)	0.260(1)	0.113(9)	0.559(2)
N(1)	0.964(2)	0.525(5)	0.260(1)	0.113(9)	0.441(2)
Rb(2)	0.483(2)	1.009(3)	0.761(1)	0.057(2)	0.559(2)
N(2)	0.483(2)	1.009(3)	0.761(1)	0.057(2)	0.441(2)
O(1)	0.191(2)	1.010(7)	0.531(1)	0.085(6)	1
O(2)	1.047(5)	0.929(5)	0.380(5)	0.140(2)	1
O(3)	0.592(4)	0.612(6)	0.110(3)	0.120(1)	1
O(4)	0.568(5)	0.645(5)	0.905(5)	0.088(6)	1
O(11)	0.118(4)	1.010(1)	0.845(3)	0.128(9)	1
O(12)	1.016(5)	1.210(5)	0.872(5)	0.130(4)	1
O(13)	1.122(3)	0.254(5)	0.084(2)	0.086(6)	1
O(21)	0.714(2)	0.618(4)	0.436(2)	0.076(5)	1
O(22)	0.579(3)	0.809(6)	0.507(3)	0.105(8)	1
O(23)	1.367(3)	0.487(4)	0.328(1)	0.080(9)	1
H(1)	1.0729	0.5345	0.2200	0.050	1
H(2)	1.0487	0.6296	0.2400	0.050	1
H(3)	0.9563	0.6312	0.3400	0.050	1
H(4)	0.8300	0.5364	0.2600	0.050	1
H(5)	0.5716	1.0346	0.7200	0.050	1
H(6)	0.5495	1.1260	0.7400	0.050	1
H(7)	0.4534	0.1304	0.8400	0.050	1
H(8)	0.4730	1.0028	0.5882	0.050	1
H(11)	0.1638	1.0306	0.9400	0.050	1
H(12)	1.0597	0.2939	0.0800	0.050	1
H(13)	1.2136	0.2780	0.1600	0.050	1
H(21)	0.3354	0.5308	0.5600	0.050	1
H(22)	0.4044	0.7790	0.5600	0.050	1
H(23)	0.4530	0.4143	0.3200	0.050	1

Note. $U_{eq} = 1/3 \sum_i \sum_j U_{ij}\, a_i^* a_j^* a_i a_j$.
Standard deviations are in parentheses.

Differential scanning calorimetry (DSC) was performed with a DSC SETARAM 92 between 300 and 750 K. The crystal used for the structure determination had a size of about $(0.29 \times 0.25 \times 0.14)\,mm^3$. The intensity data were recorded on an Enraf–Nonius Kappa CCD diffractometer equipped with Mo$K\alpha$ radiation (9). Before heating the solution, we regain the cell parameters of the RNST mixed solution already found at room temperature. The unit cell parameters are identified and refined using a Denzo and collect programs (10). The integrated intensities were corrected for Lorentz and polarization effects (11). All subsequent computations were carried out using the computer program SHELX (12, 13). The structure was solved by conventional Patterson and difference-Fourier techniques and refined by the full-matrix least-squares procedure. The hydrogen atoms are calculated and fixed because at high temperature, they are disordered. The crystal data and details of data collection and refinement for the RNST material, at 435 K, are summarized in Table 1. The final positional and equivalent isotropic thermal parameters are given in Table 2.

Electrical impedances were measured in the range 100 Hz–13 MHz using a Hewlett–Packard 4192 A automatic bridge monitored by an HP vectra microcomputer.

III. RESULTS AND DISCUSSIONS

III.1. Differential Scanning Calorimetry (DSC)

DSC was performed between 300 and 750 K. Figure 1 shows the results of the DSC study for $Rb_{1.12}(NH_4)_{0.88}SO_4 \cdot Te(OH)_6$ obtained on heating the polycrystalline sample. The curve reveals three distinct endothermic peaks at 418, 482, and 517 K. The second and third ones are very strong. The calculated enthalpy for the first transition is $\Delta H_1 = 22.54\,J\,g^{-1}$. The second and the third peaks are stacked. In consequence, the third peak hides the second one. Consequently, the enthalpy for the sum of these peaks is $\Delta H_2 = 307.64\,J\,g^{-1}$. The peak at 418 K is attributed to a structural phase transition, which confirms the appearance of the polar phase at high temperature. The anomaly at 483 K, which masks another one at 458 K, is probably attributed to a superprotonic phase transition characterized by the breaking of two types of hydrogen bonds (O–H···O and N–H···O) that link TeO_6 and/or NH_4 to SO_4 and the proton becomes free between potential holes of anionic and cationic polyhedra (1, 2), whereas the peak, at about 458 K, is probably due to a ferro–paraelectric phase transition (1–4). The third peak cannot be attributed to the melting

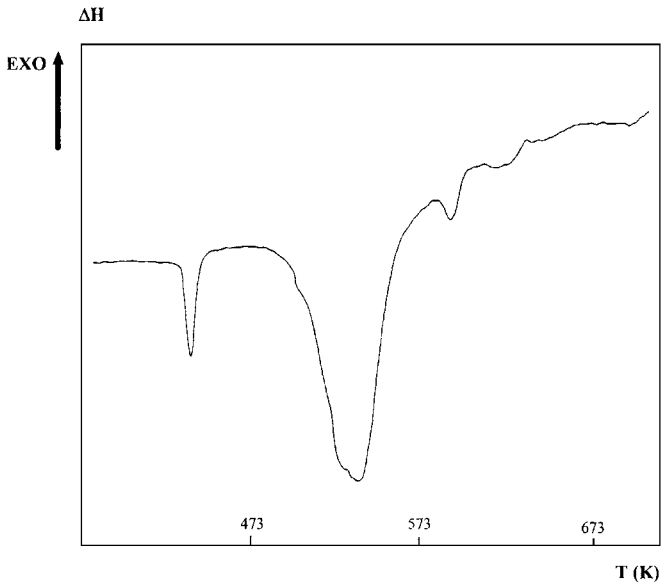

FIG. 1. Differential scanning calorimetry of $Rb_{1.12}(NH_4)_{0.88}SO_4 \cdot Te(OH)_6$.

point, because after the experiment, the material preserves its solid state. This anomaly is related to the decomposition of the salt. In consequence, the crystals change colors and become opaque. These interpretations are confirmed by the electrical studies of our solid solution.

III.2. Structural Study

To confirm our last thermal interpretations that the high-temperature phase transition detected in the DSC study at 418 K and attributed to a structural phase transition transforms our solid solution from a paraelectric to a ferroelectric one, we present in this work a structural study of the RNST material beyond the temperature phase transition. In consequence, the rubidium ammonium sulfate tellurate $Rb_{1.12}(NH_4)_{0.88}SO_4 \cdot Te(OH)_6$ crystallizes, at 435 K, in the monoclinic system with space group $P2$. After this transition the crystal remains colorless and transparent.

In order to gain more information about the relationship between the two unit cell phases at room and high temperature, we have considered the following studies (17, 18). The phase transition at 418 K, detected by DSC, in our solid solution is of first-order type. Therefore it is meaningless to talk about a group–subgroup relation between the two space groups during the transition. Our crystallographic study shows that the obtained unit cell has a unit cell volume half of the one at room temperature and contains $Z = 2$ unit formulas. Also the crystallographic b axis remains unchanged at the phase transition. In the case of the phase transition at 418 K being of second order, the mid-temperature structure (at 435 K) of our mixed compound will posses an orthorhombic lattice, and the phase transition occurs at the Brillouin zone of the orthorhombic lattice of the high-temperature phase. In our case the structure transits from the monoclinic space group $P2_1/a$ to the $P2$ one with a β angular deviation from the orthorhombic symmetry ($\beta = 98.03°$). This fact can be the consequence of the first-order character of the phase transition at 418 K. This behavior can explain the decreasing of the symmetry at high temperature of our material.

At 435 K, the RNST mixed compound shows a structural arrangement that is different from that obtained at room temperature. As reported in a previous work, RNST material crystallizes at 293 K in monoclinic symmetry, space group $P2_1/a$. The structure can be regarded as being built of planes of pure SO_4 tetrahedra and pure TeO_6 octahedra alterning with Rb^+ and NH_4^+ cations statistically disordered on one atomic position. All these planes are parallel to the bc one (Fig. 2). At 435 K, the structure is formed by planes of mixed polyhedra: octahedra of TeO_6 and tetrahedra of SO_4, parallel to the bc plane, and the Rb^+/NH_4^+ cations assure the cohesion between them. In a direction parallel to $(a + c, b)$, we observe parallel planes of pure SO_4 tetrahedra alternating with pure planes of TeO_6 octahedra and the cations also are intercalated between them. A projection of this structure on the ab plane, at 435 K, is depicted in Fig. 3. The main interatomic distances and bond angles with estimated standard deviations derived from the refinement are given in Table 3.

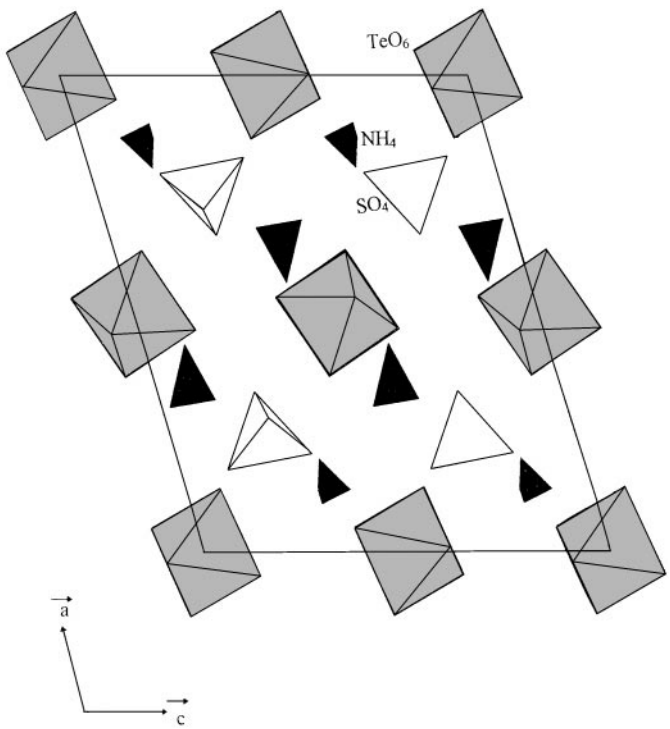

FIG. 2. Projection of $Rb_{1.12}(NH_4)_{0.88}SO_4 \cdot Te(OH)_6$ crystal structure at 293 K on the ac plane.

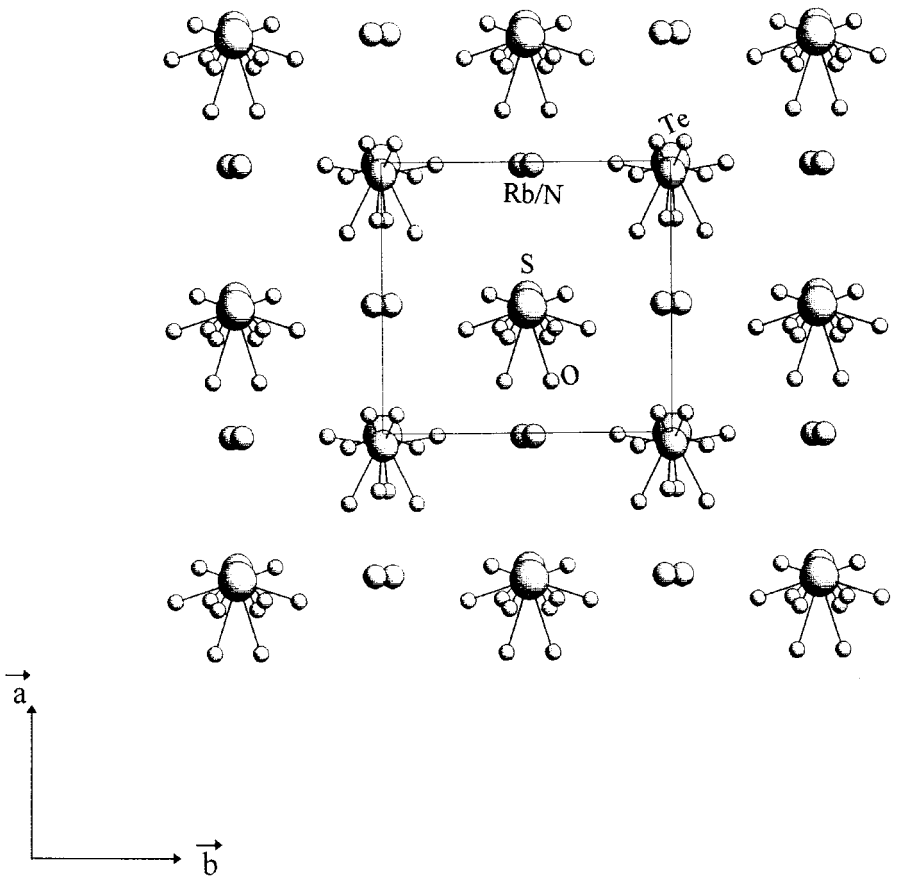

FIG. 3. Projection of $Rb_{1.12}(NH_4)_{0.88}SO_4 \cdot Te(OH)_6$ crystal structure at 435 K on the *ab* plane.

Like at the room temperature, at 435 K, the Te atoms occupy two different positions with 0.5 occupancy run. The site symmetries, in the second phase, correspond to the binary axis site, whereas in the first one they correspond to a center of inversion. In consequence, the structure shows two types of octahedra. The $Te(1)O_6$ octahedra have two Te(1)–O distances of 1.91(3) Å, two bond lengths of 2.06(3) Å, and two others of 1.92(2) Å, and O–Te(1)–O angle values vary from 81.3(26)° to 126.1(29)°. The second type of $Te(2)O_6$ octahedra have two Te(2)–O distances of 1.90(2) Å and four others of 1.91(3) Å. The O–Te(2)–O angle values are between 89.9(11)° and 110.0(13)°. In consequence, under the effects of the temperature, the oxygen atoms are more restless at 435 K than at room temperature, which is a part of the origin of the deformation of these octahedra. Indeed, at 293 K, the Te–O distances of TeO_6 octahedra are between 1.904(3) and 1.925(2) Å, whereas at 435 K, they spread from 1.90(2) to 2.06(3) Å. The O–Te–O angle values vary from 88.1(2)° to 91.9(2)° at 293 K and from 81.3(26)° to 126.1(29)° at high temperature.

In contrast with the sulfates studied, this structure presents two types of tetrahedra of SO_4. The sulfur atoms occupy binary axis sites, whereas at room temperature they are in general positions. The first type of tetrahedra $S(1)O_4$ shows two distances of S(1)–O at 1.45(2) Å and two others at 1.52(7) Å, whereas in the second type of tetrahedra $S(2)O_4$, we found two S(2)–O distances of 1.46(4) Å and two bond lengths of 1.52(2) Å. An interesting point is that, compared with the room temperature structure where the O–S–O angles are on average 109°, the SO_4 tetrahedra here are distorted with O–S–O angles varying from 75.8(11)° to 94.9(12)°. This difference can explain the disordered state at high temperature.

The Rb/N atoms are distributed on two sites. In one of them, the Rb/N atom is coordinated by three oxygen atoms belonging to SO_4 tetrahedra, two belonging to $Te(1)O_6$ octahedra, three belonging to $Te(2)O_6$ octahedra, and one belonging to another $Te(2)O_6$ octahedra. In the second site, two oxygen atoms belonging to SO_4 tetrahedra, three belonging to $Te(1)O_6$ octahedra, one belonging to another $Te(1)O_6$ octahedra, and only two belonging to $Te(2)O_6$ octahedra participate in the Rb(2) coordination, reducing the coordination number of this Rb/N atom to 8. The Rb–O distances vary from 2.54(3) to 3.62(10) Å for the first rubidium/ammonium atom, whereas they are between 2.90(2) and 3.58(3) Å for the second cation. In the room temperature

TABLE 3
Atomic Distances (Å) and Angles (°) of $Rb_{1.12}(NH_4)_{0.88}SO_4 \cdot Te(OH)_6$

(a) Rubidium and ammonium coordination

Rb(1)/N(1)	Rb(2)/N(2)
O(12) e … 2.54 (3)	O(4) … 2.90 (2)
O(21) … 2.84 (3)	O(1) … 2.98 (2)
O(13) … 2.93 (4)	O(11) … 2.99 (4)
O(2) … 3.02 (3)	O(22) p … 3.03 (3)
O(23) … 3.03 (3)	O(3) p … 3.07 (4)
O(3) … 3.06 (4)	O(22) … 3.09 (3)
O(11) p … 3.55 (10)	O(21) p … 3.53 (3)
O(11) d … 3.62 (10)	O(13) b … 3.56 (3)
	O(23) b … 3.58 (3)

(b) Sulfate groups

S(1)–O(1) g = 1.45 (2)	O(1) g–S(1)–O(2) a = 94.9 (12)
S(1)–O(1) f = 1.45 (2)	O(1) f–S(1)–O(2) a = 75.8 (11)
S(1)–O(2) a = 1.52 (7)	O(1) g–S(1)–O(2) d = 76.0 (11)
S(1)–O(2) d = 1.52 (7)	O(1) f–S(1)–O(2) d = 94.7 (12)
S(2)–O(3) = 1.46 (4)	O(3)–S(2)–O(4) p = 48.3 (17)
S(2)–O(3) h = 1.46 (4)	O(3) h–S(2)–O(4) p = 87.8 (22)
S(2)–O(4) p = 1.52 (2)	O(3)–S(2)–O(4) k = 88.0 (22)
S(2)–O(4) k = 1.52 (2)	O(3) h–S(2)–O(4) k = 48.2 (17)
	O(11) l–Te(1)–O(12) d = 126.1 (29)
	O(11)g–Te(1)–O(12) c = 126.1 (29)
	O(11) g–Te(1)–O(13) m = 81.3 (26)
	O(11) l–Te(1)–O(13) m = 93.3 (26)
	O(11) g–Te(1)–O(13) h = 93.2 (26)
	O(11) l–Te(1)–O(13) h = 81.3 (26)

(c) Tellurate groups

Te(1)–O(11) g = 1.91 (3)	O(21) p–Te(2)–O(22) = 90.2 (13)
Te(1)–O(11) l = 1.91 (3)	O(21)–Te(2)–O(22) p = 90.3 (13)
Te(1)–O(12) d = 1.92 (2)	O(21)–Te(2)–O(23) m = 96.1 (10)
Te(1)–O(12) c = 1.92 (2)	O(21) p–Te(2)–O(23) m = 89.9 (11)
Te(1)–O(13) m = 2.06 (3)	O(22)–Te(2)–O(23) m = 109.7 (13)
Te(1)–O(13) h = 2.06 (3)	O(22) p–Te(2)–O(23) m = 91.2 (12)
Te(2)–O(21) = 1.90 (2)	O(21)–Te(2)–O(23) n = 89.9 (11)
Te(2)–O(21) p = 1.90 (2)	O(21) p–Te(2)–O(23) n = 96.2 (10)
Te(2)–O(22) = 1.91 (3)	O(22)–Te(2)–O(23) n = 91.5 (12)
Te(2)–O(22) p = 1.91 (3)	O(22) p–Te(2)–O(23) n = 110.0 (13)
Te(2)–O(23) m = 1.91 (2)	
Te(2)–O(23) n = 1.91 (2)	
O(11)–H(11) = 0.97 (5)	
O(12)–H(12) = 0.97 (5)	
O(13)–H(13) = 0.97 (5)	
O(21)–H(21) = 0.71 (5)	
O(22)–H(22) = 0.73 (5)	
O(23)–H(23) = 0.82 (5)	

Note. See Table 4 for symmetry codes.

structure, the two rubidium cations are nine coordinated and the Rb–O distances vary from 2.89(3) to 3.28(3) Å.

In RNST structure, at 435 K, the sulfate tetrahedra are connected with tellurate octahedra by hydrogen bonds O–H···O assured by protons belonging to (OH^-) groups. In consequence, two oxygen atoms O(4) and O(3) belonging to the $S(2)O_4$ group participate in the formation of this type of bond, each one linked to O(23), with O···O distances of respectively 2.71(2) and 3.08(4) Å. These values are slightly more longer than those found at 293 K (2.68(4)–2.79(4) Å). In addition to O–H···O hydrogen bonding, the structure of this mixed compound is characterized by N–H···O bonds. As seen in Table 4, and in contrast with the room temperature structure, where only one hydrogen atom linked to N(1) participates in the formation of this type of hydrogen bonding, at 435 K, all hydrogen atoms linked to N(1) participate in the formation of N–H···O bonding with O···H distances ranging from 2.18(2) to 2.47(1) Å. Three hydrogen atoms bonded to N(2) contribute in the formation of N–H···O bonds with distance values varying from 2.12(2) to 2.64(3) Å. The N–H···O angles spread from 95.39(2)° to 136.61(1)° but at room temperature, they vary from 128.2(1)° to 150.9(1)° and the O···H distances are between 2.25(3) and 2.47(3) Å. The large difference between the O···O and O···H···O angle values in the two different structures is related to the effect of the temperature where the protons H^+ are very disordered.

The results observed in the high-temperature structural study show clearly the important changes in the arrangement and confirm the presence of the phase transition detected in the DSC curve at 418 K.

III.3. Electrical Properties

Polycrystalline pellets, 13 mm in diameter and 1 mm in thickness, were obtained, at room temperature, under 200 MPa stress. The pellets were sintered at 420 K for 12 h in vacuum. This processing was applied to eliminate, as much as possible, the water content in the sample and to obtain dense pellets.

Complex impedance diagrams $Z''(\Omega)$ as a function of $Z'(\Omega)$, i.e., Cole–Cole plots (14), are presented in Fig. 4 for $Rb_{1.12}(NH_4)_{0.88}SO_4 \cdot Te(OH)_6$ at various temperatures. The bulk ohmic resistance corresponding to each experimental temperature is the intercept on the real axis of zero phase angle extrapolation of the highest-frequency curve (15).

The temperature dependence of the conductivity is represented in Fig. 5 in a $\log(\sigma T)$ vs $1/T$ plot. An Arrhenius-type behavior was observed in the temperature range 450–500 K. The diagram, in Fig. 5, exhibits two regions: (a) the first one above 482 K has an arc form and the conductivity does not obey the Arrhenius law. This phenomenon can be due to the superposition of many mechanisms such as the breaking of the hydrogen bonds, the reorientation of the ammonium tetrahedra, and the beginning of the decomposition of the salt. (b) The second one below 482 K with a jump characterizes the protonic conduction phase transition of the salt. The conductivity plot, in this region, exhibits two parts with a transition at 450 K, which can be attributed to the ferroelectric–paraelectric phase transition. The activation energies of the two parts are respectively $\Delta E_1 = 0.59$ eV and $\Delta E_2 = 1.44$ eV. The difference and the larger of the

TABLE 4
Distances and Hydrogen Bond Angles in $Rb_{1.12}(NH_4)_{0.88}SO_4 \cdot Te(OH)_6$

O..O and N..O distances (Å)	O..H distances (Å)	O..H–O and O..N–H angles (°)
O–H … O bonds		
O(3) … O(23) m = 3.08 (4)	O(3) … H(23) = 2.83 (3)	O(3) … H(23)-O(23) m = 99.85 (2)
O(4) … O(23)n = 2.71 (2)	O(4) … H(23) p = 2.76 (1)	O(4) … H(23)p–O(23)n = 78.19 (2)
N–H … O bonds		
N(2) … O(1) = 2.98 (2)	O(1) … H(8) = 2.12 (2)	N(2)–H(8) … O(1) = 100.15 (9)
N(2) … O(11) = 2.99 (3)	O(11) … H(7) = 2.63 (3)	N(2)–H(7) … O(11) = 95.39 (2)
N(2) … O(22) = 3.09 (3)	O(22) … H(5) = 2.64 (3)	N(2)–H(5) … O(22) = 113.62 (1)
N(1) … O(2) = 3.02 (3)	O(2) … H(2) = 2.47 (1)	N(1)–H(2) … O(2) = 114.03 (1)
N(1) … O(3) = 3.06 (3)	O(3) … H(4) = 2.24 (3)	N(1)–H(4) … O(3) = 136.61 (1)
N(1) … O(13) = 2.93 (3)	O(13) … H(1) = 2.40 (3)	N(1)–H(1) … O(13) = 113.78 (2)
N(1) … O(21) = 2.84 (3)	O(21) … H(3) = 2.18 (2)	N(1)–H(3) … O(21) = 116.48 (1)
N(1) … O(23) = 3.03 (2)	O(23) … H(1) = 2.36 (2)	N(1)–H(1) … O(23) = 125.87 (1)

Note. Symmetry code: a: $x-1, y-1, z$; b: $-x+2, y+1, -z+1$; c: $x-1, y-1, z-1$; d: $-x+1, y-1, -z+1$; e: $-x+2, y-1, -z+1$; f: $x, y-1, z$; g: $-x, y-1, -z+1$; h: $-x+1, y, -z$; k: $x, y, z-1$; l: $x, y-1, z-1$; m: $x-1, y, z$; n: $-x+2, y, -z+1$; p: $-x+1, y, -z+1$.

activation energies for a typical superprotonic conductor can be due to the difficulty of the proton displacement caused by the cell deformation introduced with the establishment of a polar phase. In the RNST structure SO_4^{2-}, NH_4^+, and TeO_6^{6-} group are connected by hydrogen bonds. In consequence, the transition at 482 K, observed in DSC at the same temperature, is characterized by the breaking of these hydrogen bonds, and the proton becomes free as the potential hole reaches the "quasi-liquid" state where the proton and the SO_4^{2-} and TeO_6^{6-} ions contribute to the unusually high conductivity as in the case of $CsHSO_4$ (16).

Figure 6 illustrates the temperature dependence of the permittivity ε'_r in the range 400–600 K for RNST material. This curve shows two anomalies at about 458 and 487 K attributed to the phase transitions detected by DSC. The permittivity ε'_r around T_1 and T_2 increases considerably as the frequency decreases. This is in agreement with the contribution of the conductivity in this material. The first anomaly characterizes the ferroelectric–paraelectric phase transition, whereas the second one is attributed to the superprotonic conduction. This interpretation was confirmed by our last relaxation study, which shows that the maximum of

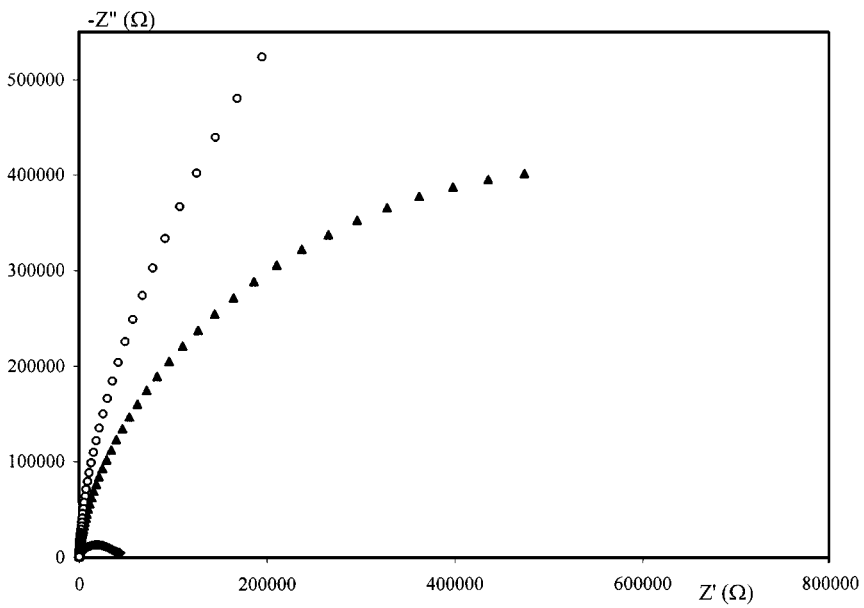

FIG. 4. Complex impedance curves of the mixed compound $Rb_{1.12}(NH_4)_{0.88}SO_4 \cdot Te(OH)_6$ at various temperatures. T = 403 (○), 429 (▲), and 458 K (◆).

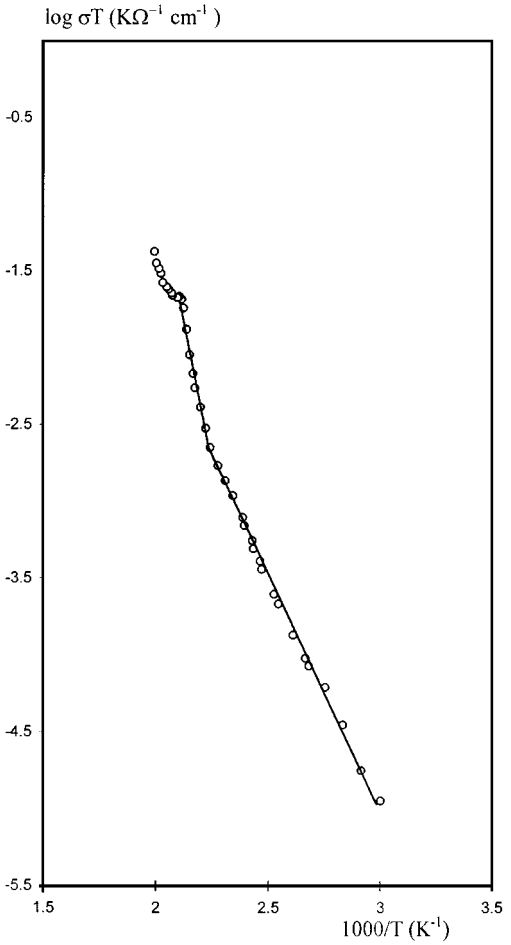

FIG. 5. Conductivity plot log $(\sigma T) = f(10^3/T)$ for $Rb_{1.12}(NH_4)_{0.88}SO_4 \cdot Te(OH)_6$.

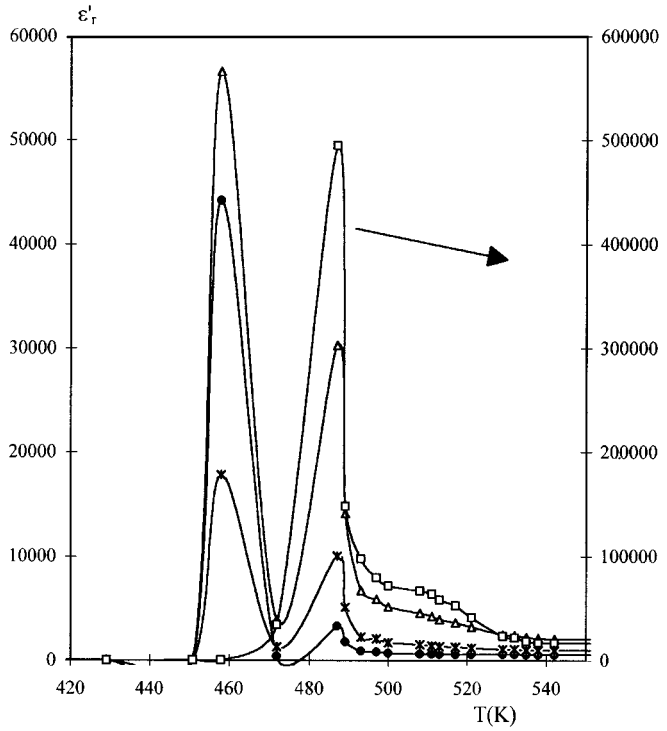

FIG. 6. Temperature dependence of ε'_r as a function of frequency for $Rb_{1.12}(NH_4)_{0.88}SO_4 \cdot Te(OH)_6$. $f = 0.1$ (□), 1 (△), 3 (∗), and 10 KHz (●).

the permittivity at 458 K is accompanied by a minimum of the dissipation factor at the same temperature characterizing the ferroelectric–paraelectric phase transition (1, 2, 8). The maximum of the permittivity curve at 487 K is displaced to higher temperature with increasing frequency, which is in agreement with the presence of conductivity relaxation. In consequence, the real part of the permittivity can be considered as the sum of two contributions,

$$\varepsilon'_r = \varepsilon'_r(\text{latt.}) + \varepsilon'_r(\text{carr.}),$$

where ε'_r(latt.) and ε'_r(carr.) represent respectively the lattice response due to permanent dipole orientation and the charge carrier response associated with long-range migration.

IV. CONCLUSION

The interesting aspect of this structure is the presence of two different anions SO_4^{2-} and TeO_6^{6-} in the same crystal, which can be the cause of the appearance of the ferroelectric phase in this type of material. The structure of RNST at high temperature crystallizes in the monoclinic system with *P*2 space group, showing a structural arrangement that is different from that obtained at room temperature. The structure can be regarded as being built of planes of mixed polyhedra: alternating TeO_6 octahedra and SO_4 tetrahedra parallel to *bc* plane, with Rb^+/NH_4^+ cations assuring the cohesion of the edifice. The RNST structure is stable thanks to two types of hydrogen bonds O–H···O and N–H···O. A preliminary electric study shows that the presence of these hydrogen bonds is part of the origin of the superprotonic phase transition due to the breaking of the hydrogen bonds, and appears as a strong jump in the conductivity plot at about 482 K.

The high-temperature structural study confirms that the phase transition, detected at 418 K in the DSC, can be considered as a mixed phase between two symmetric paraelectric phases, and the space group becomes the non centrosymmetric *P*2, which can favor the high-temperature polar phase and confirm our electrical study that the RNST material is ferroelectric in a temperature range between 418 and 458 K.

ACKNOWLEDGMENT

We express our thanks to Dr. R. Ben Hassen for his fruitful discussions and crystallographic interpretations.

REFERENCES

1. M. Dammak, H. Khemakhem, N. Zouari, T. Mhiri, and A. W. Kolsi, *Solid State Ionics* **127,** 125 (2000).
2. Z. Czapla and G. Pykach, *Bull. Acad. Sci. USSR Phys. Ser.* (*USA*) **55,** 22 (1991); Translation of *Izv. Akad. Nauk SSSR Ser. Fiz.* (*USSR*) **55,** 439 (1991).
3. S. Guillot Gauthier, J. C. Peuzin, M. Olivier, and G. Rolland, *Ferroelectrics* **52,** 293 (1984).
4. H. Khemakhem, *Ferroelectrics* **234,** 47 (1999).
5. M. Dammak, H. Khemakhem, T. Mhiri, A. W. Kolsi, and A. Daoud, *J. Alloys Compds.* **280,** 107 (1998).
6. R. Zilber, A. Durif, and M. T. Averbuch-Pouchot, *Acta Crystallogr. Sect. B* **37,** 650 (1981).
7. L. Ktari, M. Dammak, T. Mhiri, and A. W. Kolsi, submitted for publication.
8. L. Ktari, M. Dammak, T. Mhiri, and A. W. Kolsi, *in* "Proceeding of the SSPC 10, Montpellier 2000," p. 120.
9. Nonius, Kappa CCD Server Software, Nonius B. V. Delft, The Netherlands (1997).
10. R. Hooft, "Collect" data collection software, Nonius B. V. (1998).
11. A. C. T. North, D. C. Philips, and F. S. Mattews, *Acta Crystallogr. Sect. A* **39,** 351 (1968).
12. G. M. Sheldrick, "SHELXS 86, Program for the Solution of Crystal Structures." University of Göttingen, Göttingen, Germany, 1990.
13. G. M. Sheldrick, "SHELXL 93, Program for Crystal Structure Determination." University of Göttingen, Göttingen, Germany, 1993.
14. K. S. Cole and R. H. Cole, *J. Chem. Phys.* **43,** 341 (1941).
15. J. F. Bauerle, *J. Phys. Chem.* **30,** 2657 (1969).
16. N. G. Hainovsky and E. Hairetdinov, *Izv. Ot. SSSR Ser. Khim. Nauk* **8,** 33 (1985).
17. H. Smaoui, H. Guermazi, Y. Mlik, and T. Mhiri, *Eur. Phys. J. AP* **11,** 83 (2000).
18. K. Aizu, *J. Phys. Soc. Jpn.* **36,** 937 (1974).